Research Square

Preprints are preliminary reports that have not undergone peer review.
They should not be considered conclusive, used to inform clinical practice,
or referenced by the media as validated information.

Cassava root rots in the humid tropics: fungal niche inversion and early-warning threshold in West Africa

Arthur Martin AFFERY

arthuraffery@yahoo.fr

Université de Man https://orcid.org/0000-0001-9644-7605

Arthur Martin Affery
Yaya Toure
Yao Firmin N'Guessan
Acka Emmanuel Dick

Research Article

Keywords: Manihot esculenta, Sclerotium rolfsii, Lasiodiplodia theobromae, fungal niche inversion, topographic risk inversion, Côte d'Ivoire

Posted Date: October 5th, 2026

DOI: https://doi.org/10.21203/rs.3.rs-10863755/v1

License: This work is licensed under a Creative Commons Attribution 4.0 International License.
Read Full License

Additional Declarations:
Tables are available in the Supplementary Files section.

Cassava root rots in the humid tropics: fungal niche inversion and early-warning threshold in West Africa

Arthur Martin Affery[1], Yaya Toure[1], Yao Firmin N'Guessan[1] and Acka Emmanuel Dick[2]

[1] Universite de Man, UFR Ingenierie agronomique, forestiere et environnementale (UFR-IAFE), BP 20, Man, Cote d'Ivoire.

[2] Universite Felix Houphouet-Boigny, UFR Biosciences, Laboratoire de physiologie vegetale, 22 BP 582 Abidjan 22, Cote d'Ivoire.

Corresponding author: Arthur Martin Affery; E-mail: arthuraffery@yahoo.fr

Abstract

Cassava (*Manihot esculenta* Crantz) root rots, caused by soil-borne fungi, constitute a major constraint in the West African humid tropics. However, their combined effects with topography, altitude and plant age remain insufficiently documented. This study evaluated these effects via the Disease Severity Index (DSI) across 192 plots and 1,920 plants aged 8–25 months, in three contrasting regions (Tonkpi, Guémon, Cavally) of the mountainous west of Côte d'Ivoire. An early-warning threshold (DSI > 0.5, i.e. 12.5% on the proportional scale), derived from the inflection of the age–severity curves, was retained as the operational benchmark marking entry into the active epidemic phase. The marketable-yield deficit was estimated on the basis of 10 t ha^{-1}. The Cavally lowlands (< 200 m) exhibited the highest disease levels (prevalence = 81.5%; DSI = 2.00 ± 1.33) and an estimated marketable deficit of 4.32 t ha^{-1}. These plots were dominated by *Sclerotium rolfsii* (98.2% of infection profiles), alone or in co-infection with *Lasiodiplodia theobromae*, with the early-warning threshold crossed as early as 8 months after planting. Conversely, the hydromorphic Tonkpi lowlands (> 300 m) exhibited reduced severity

(DSI = 0.81 ± 1.19) and a dominance of *Lasiodiplodia theobromae* (94.3%). An estimated thermal difference of 1–2 °C, derived from the adiabatic lapse rate (−0.65 °C per 100 m), reverses fungal dominance in the lowlands, illustrating a 'fungal niche inversion'. The Cavally summits (DSI = 0.46 ± 0.79) sustained higher pathogen pressure than the Tonkpi slopes (DSI = 0.23 ± 0.53), revealing a 'topographic risk inversion'. These two phenomena demonstrate that topography, altitude and physiological age cannot be disentangled in risk assessment. These results provide a spatial decision-making grid to guide phytosanitary surveillance and to adapt harvest calendars in the humid tropics.

Keywords: *Manihot esculenta*; *Sclerotium rolfsii*; *Lasiodiplodia theobromae*; fungal niche inversion; topographic risk inversion; Côte d'Ivoire

1. Introduction

Cassava (*Manihot esculenta* Crantz) is a major staple crop in sub-Saharan Africa, where it contributes to food security and to the incomes of millions of rural households (Hillocks et al., 2002; FAO, 2023). In Côte d'Ivoire, this importance is magnified by its local processing, notably through the production of *attiéké*, a fermented semolina whose associated know-how ('Attiéké des lagunes') was inscribed on the UNESCO Representative List of the Intangible Cultural Heritage of Humanity in 2024 (UNESCO, 2024). The sustainability of this label of excellence, however, depends on the production of healthy tubers, which is currently compromised by crop intensification and the expansion of cultivated areas into hydromorphic lowlands. These agrarian dynamics favour the destructive emergence of soil-borne root rots (Banito et al., 2010; Zinsou et al., 2017). Primarily associated with *Lasiodiplodia theobromae* and *Sclerotium rolfsii*, these infections cause progressive necrosis of root tissues and can lead to substantial yield losses, sometimes exceeding 80% in the most permissive pedoclimatic contexts (Vilas Boas et al., 2017; Sangpueak et al., 2023).

Despite the magnitude of these losses, the epidemiology of these diseases has hitherto been addressed in a fragmented manner. Plant physiological age is often used as a chronological harvest benchmark, with a practical threshold set at around 12 months after planting (Onyeka et al., 2005b). In parallel, soil waterlogging induces hypoxic stress that weakens root defences and favours the development of soil-borne fungi (Zinsou et al., 2017; Sangpueak et al., 2023). However, the combined effects of plant age, regional altitude and topographic position remain insufficiently documented. This gap raises a central question: how does the interaction between regional altitude, topographic position and plant physiological age influence the severity of root rots? A single-factor approach may thus mask the risk combinations observed at the landscape scale and prevent the contextualisation of intervention thresholds. This need to spatialise risk makes it essential to define a DSI-based early-warning threshold in order to anticipate harvest before any irreversible commercial loss occurs.

The Montagnes District, in western Côte d'Ivoire, provides a relevant natural setting in which to address this question. This territory combines a marked altitudinal gradient, ranging from the mountainous zones of Tonkpi to the lowlands of Cavally, and local toposequences extending from well-drained summits to hydromorphic lowlands. This configuration allows the joint analysis of the effects of regional altitude, local topographic position and plant age on the expression of root rots. It thus provides the opportunity to study the spatial structuring of epidemic risk at the landscape scale (Ostfeld et al., 2005), whilst examining the restructuring of fungal niches along elevational gradients (Lin et al., 2024).

To update surveillance strategies in the humid tropics, the present study addresses this issue by pursuing three objectives: (i) to quantify the combined effects of topography, altitude and age on the incidence and severity of root rots; (ii) to characterise the variation in fungal-complex composition along this dual hydrothermal gradient; and (iii) to estimate, from the age–severity

curves, the age at which a DSI-based early-warning threshold marking entry into the active epidemic phase is crossed, in order to develop a spatial decision-making grid to optimise surveillance and harvest calendars.

2 Materials and methods

2.1 Study area and sampling design

The study was conducted in the Montagnes District, western Côte d'Ivoire. This zone is characterised by a marked altitudinal gradient (158–790 m) and by a bimodal annual rainfall of 1,600–2,000 mm, favourable to the development of soil-borne pathogens (Zinsou et al., 2017). The design covered three contrasting administrative regions: Tonkpi, a highland zone (233–790 m); Guémon, a hilly zone (204–368 m); and Cavally, a low-altitude alluvial plain (158–293 m).

A stratified sampling scheme based on the Region × Toposequence interaction was implemented to jointly analyse the effects of regional altitude and local topographic position. Field surveys were conducted during the rainy season, from May to November 2025. A total of 192 maturing cassava plots were georeferenced using a GPS with ± 3 m accuracy. Plots were at least 5 km apart, an empirical distance judged sufficient to limit spatial dependence between observations given field accessibility constraints. Each plot was assigned to one of three topographic positions: summit/plateau, with rapid drainage; slope/mid-slope, with moderate drainage; and lowland, with frequent hydromorphy.

The number of plots per stratum was not strictly balanced between regions, owing to accessibility constraints and plot availability at the time of the surveys. The distribution was as follows: Tonkpi, 29 summits, 28 slopes and 28 lowlands; Guémon, 23 summits, 22 slopes and 23 lowlands; Cavally, 13 plots per topographic position. The topographic classification was validated in the field by observing drainage, landscape position and the potential presence of surface waterlogging.

The regional temperature of each stratum was approximated by a standard adiabatic lapse rate of −0.65 °C per 100 m of altitude (ICAO, 1993), taking as macroclimatic reference temperature T_0 = 27 °C at sea level, a value characteristic of the Ivorian coastal zone (SODEXAM, 2021; 1990–2020 mean data).

2.2 Phytosanitary assessment and disease quantification

In each smallholder plot, 10 plants were selected along a W-shaped transect (Onyeka et al., 2005b), giving a total of 1,920 plants assessed. The plant material consisted of local, genetically uncharacterised cultivars known under vernacular names. Plant age, expressed in months after planting (MAP), ranged from 8 to 25 months. It was collected through semi-structured interviews with growers and verified by cross-checking against available planting dates to limit reporting bias. Root necrosis severity was assessed on a 0–4 ordinal scale adapted from Hohenfeld et al. (2022): 0 = healthy roots; 1 = 1–25% of root surface affected; 2 = 26–50%; 3 = 51–75%; 4 = > 75% or complete destruction. The number of tuberised roots scored per plant varied from 2 to 12 (mean 6.1; median 6), giving a total of 11,697 roots assessed. The type of rot (dry, soft or mixed) was recorded in the field according to standardised visual criteria (Ferreira et al., 2019).

The Disease Severity Index (DSI) was calculated according to the principle of McKinney (1923), first at plant level and then aggregated at plot level. For a plant or a plot, the proportional form was calculated as follows:

$$\mathrm{DSI}(\%) = \frac{\sum(n_i \times v_i)}{N \times V} \times 100$$

where n_i is the number of roots in severity class i, v_i the numerical value of that class, N the total number of roots assessed and V the maximum score of the scale (4).

In the descriptive tables and figures, severity is reported as the mean score, denoted DSI (0–4). For the sole purposes of inferential modelling (GLMM), this index was converted to a continuous scale, denoted proportional DSI (0–1), by dividing the score by 4, i.e. DSI (score 0–4) = 4 × proportional DSI. For the sake of readability, the term DSI hereafter designates the raw index on the 0–4 scale, whereas 'proportional DSI' is reserved for the continuous 0–1 variable used in the GLMM.

The Root Infection Rate (RIR, %) was calculated as the proportion of roots exhibiting visible necrosis:

$$\text{RIR} = \frac{\text{n}_\text{r}}{N} \times 100$$

where n_r is the number of roots exhibiting rot symptoms and N the total number of roots examined.

RIR was used to estimate the proportion of non-marketable tubers. The reference yield potential was set at 10 t ha^{-1}, a conservative value corresponding to mean yields observed in traditional smallholder systems (low inputs) in West Africa (FAO, 2023). The estimated loss of marketable yield was calculated as follows:

$$\text{Estimated loss (t ha}^{-1}\text{)} = \frac{RIR}{100} \times 10$$

An economic warning threshold of 1 t ha^{-1} of loss (i.e. 10% of the reference potential) was adopted as the limit of commercial viability: beyond this margin, prolonging standing storage is no longer compensated by the gain in marketable tubers. This conventional value is of the order of the profitability margins observed in smallholder systems (FAO, 2023).

2.3 Preliminary morpho-cultural identification of fungal agents

For each lesion morphotype, tissue fragments were sampled from the advancing margin of the necroses. After surface disinfection in 1% sodium hypochlorite for 3 min, fragments were rinsed three times in sterile distilled water and plated on potato dextrose agar (PDA) supplemented with chloramphenicol (50 mg L^{-1}). Plates were incubated at 25 ± 2 °C in the dark for 7 days. Isolate identification relied on a morpho-cultural approach combining macroscopic observation of colonies (texture, pigmentation and growth rate) with microscopic examination of reproductive structures at ×400 (Leslie & Summerell, 2006; Crous et al., 2009). The diagnostic criteria retained were: *Sclerotium rolfsii*, silky white mycelium and spherical dark-brown sclerotia; *Lasiodiplodia theobromae*, greyish to blackish mycelium and pycnidia containing striated bilocular conidia with a central septum at maturity.

2.4 Statistical analysis and epidemiological modelling

Data analysis respected the hierarchical structure of the design (root, plant, plot). Non-parametric comparisons of severity were conducted on plot means (n = 192) to guarantee strict independence of sampling units and to avoid pseudo-replication bias. The Kruskal–Wallis test was applied with the correction for ties, followed by Dunn's post hoc tests with Bonferroni correction for multiple comparisons.

Epidemiological inference was then modelled at plant level (n = 1,920). The effects of altitude, toposequence and their interaction on proportional DSI (0–1) were evaluated by a zero-inflated beta generalised linear mixed model (ZOIB GLMM). The zero-inflation component was introduced to account for the excess of asymptomatic plants (DSI = 0), whilst the Smithson–Verkuilen transformation (Smithson & Verkuilen, 2006) adjusted for extreme values (DSI = 1).

To prevent pseudo-replication and capture intra-site spatial correlation, the factor "Plot" was included as a random intercept.

The temporal dynamics of the disease were fitted by second-degree polynomial regression, this form having been retained on the basis of the Akaike information criterion (AIC) and the adjusted R^2 after comparison with linear, exponential and logistic fits. The onset of the active epidemic phase was defined by the crossing of the operational benchmark DSI (score 0–4) > 0.5 (i.e. 0.125 in proportion). The strength of the age–severity coupling was quantified by Spearman's rank correlation coefficient (ρ), and the entropy of the fungal complex by the Shannon–Wiener index (H'). The significance threshold was set at $\alpha = 0.05$.

Non-parametric analyses, regressions and visualisations were performed in Python 3.10 (SciPy 1.11, Pandas 2.1, Statsmodels 0.14, Matplotlib/Seaborn); the ZOIB GLMM was fitted in R 4.3.2 using the glmmTMB package (Brooks et al., 2017).

3. Results

3.1 Synergistic interaction of altitude and topography on severity

Analysis of the 192 plot means revealed a highly significant spatial structuring of root rots (Kruskal–Wallis, $H = 127.8$; $df = 8$; $p < 0.001$; $\varepsilon^2 = 0.67$). This very large effect ($\varepsilon^2 > 0.60$) confirms that the Region × Toposequence combination massively structures the distribution of the disease.

Overall, severity (DSI) increased along the toposequence, from well-drained summits to hydromorphic lowlands, independently of the region. Regional macroclimatic temperatures, approximated by the adiabatic lapse rate (−0.65 °C per 100 m; reference 27 °C at sea level), differed between the two extreme altitudinal contexts: approximately 25.5–26.0 °C in the

Cavally lowlands (< 200 m) versus 24.0–24.5 °C in those of Tonkpi (> 300 m), representing a regional thermal difference of 1.0–2.0 °C. Although small in absolute value, this regional difference of 1.0–2.0 °C is sufficient to reconfigure both the intensity of risk and the structure of the pathogen complex.

Table 1 summarises the descriptive parameters per stratum. The Cavally lowlands constituted the main epidemic focus of the design (DSI = 2.00 ± 1.33; prevalence = 81.5%). Conversely, the Tonkpi lowlands, although equally hydromorphic, exhibited significantly reduced severity (DSI = 0.81 ± 1.19; $p < 0.001$), highlighting the mitigating effect of the cooler macroclimate.

An additional contrast demonstrates the predominance of the regional effect: the Cavally summits (DSI = 0.46 ± 0.79; prevalence = 52.3%) experienced higher pathogen pressure than the Tonkpi slopes (DSI = 0.23 ± 0.53; prevalence = 31.4%). This dynamic illustrates a 'topographic risk inversion': a well-drained Cavally summit is more exposed to the disease than a Tonkpi slope, even though the latter is topographically more favourable to infection.

3.2 Restructuring of the aetiological complex and fungal niche inversion

Fungal diversity (Shannon index H′) varied from 0.219 (Tonkpi lowlands) to 0.758 (Cavally lowlands), reflecting minimal community entropy in constraining environments and maximal entropy in permissive ones (Table 2).

In the Tonkpi lowlands (approximately 24.0–24.5 °C), *Lasiodiplodia theobromae* (Fig. 1d) dominated the complex (94.3% of infection profiles), associated with slowly progressing soft-rot phenotypes. At the opposite extreme, in the hot, hydromorphic Cavally lowlands (approximately 25.5–26.0 °C), *Sclerotium rolfsii* (Fig. 1e) was involved in 98.2% of infection profiles, alone (41.6%) or in co-infection with *Lasiodiplodia theobromae* (56.6%), causing rapidly progressing soft rots leading to complete destruction of the root system (Fig. 1c), in agreement with the extreme severity levels recorded (Fig. 2a). This pronounced taxonomic

transition within the same topographic position (lowland) materialises a predominantly altitude-driven fungal niche inversion'.

In parallel, the xeric environments of the Tonkpi and Guémon summits selected stress pathogens (*Fusarium solani*, *Macrophomina phaseolina*), whose dry lesions frequently remained superficial (Fig. 1b).

3.3 Modelling of epidemic kinetics and age–severity coupling

Plant-level inference (n = 1,920) by the ZOIB GLMM confirmed the validity of this hierarchical structuring. The variance of the plot random intercept was $\sigma^2 = 0.392$ for an intra-plot residual variance of 0.600 (latent logit scale), yielding a conditional intraclass correlation (ICC) of 0.395 — a spatial aggregation that notably absorbs the between-plot component of the heterogeneity of the uncharacterised local cultivars (see Section 2.2). In the null model, this between-plot variance reached 1.427 (ICC = 0.704); the fixed effects of region, topography and age thus explained 72.5% of the between-plot variance. The necessity of the random effect was confirmed by the likelihood-ratio test ($\chi^2 = 533.7$; $p < 10^{-11}$). The fixed effects confirmed the aggravating role of the 'lowland' position ($\beta = 1.86$; $p < 0.001$) and a significant altitude × slope interaction ($\beta = -0.58$; $p = 0.019$).

Plant physiological age exacerbated this spatial vulnerability following non-linear kinetics (polynomial regressions, $R^2 > 0.78$ in the critical strata) (Fig. 3). Spearman's coefficient quantified this determinism: the age–severity coupling shifted from a loose relationship on the

protective Tonkpi summits ($\rho = 0.212$) to a very strong monotonic relationship in the Cavally lowlands ($\rho = 0.868$) (Table 3; Fig. 4a).

The onset of the active epidemic phase (crossing of raw DSI > 0.5) varied strongly along this gradient. It imposed an agronomic warning as early as 8 months after planting (MAP) in the Cavally lowlands, whereas it was never reached over the observation period (up to 25 MAP) on the Tonkpi summits, and was crossed only at 16 MAP on the slopes of the same region (Table 3). This acceleration translated into a major divergence in infection levels within the region: at comparable mean age (approximately 16 MAP), the proportion of infected plants reached 81.5% in the lowlands versus 52.3% on the summits, amounting to a difference of nearly 30 percentage points.

3.4 Agronomic impact and validation of the decision-making model

The marketable-yield deficit closely followed this geography of risk (Fig. 4). The estimated proportion of non-marketable tubers reached its highest level in the Cavally lowlands, representing an estimated marketable deficit of 4.32 t ha^{-1}, approximately 43.2% of the theoretical yield potential. Beyond 15 MAP, the proportion of non-marketable tubers reached 75.2% in these strata, rendering the crop economically non-viable according to the 1 t ha^{-1} warning threshold (Fig. 4b).

At the opposite extreme, the Tonkpi summits demonstrated remarkable sanitary resilience: the deficit was contained at 0.51 ± 0.13 t ha^{-1}, allowing safe standing storage even beyond 20 MAP. In other words, whereas harvest at 12 MAP constitutes a safe practice on the Tonkpi summits, it represents a critical delay in the Cavally lowlands, where the epidemic phase was activated

as early as 8 MAP. The stratification of these epidemiological dynamics validates the need for a spatialised decision-making model (Fig. 5) to optimise harvesting windows.

4. Discussion

In West Africa, the dynamics of cassava root rots have long been addressed in a fragmentary manner. Studies conducted in Togo (Banito et al., 2010) and Benin (Zinsou et al., 2017) established that hydromorphic soils constitute a major risk factor. The confrontation of our results with these studies, and with the seminal work of Onyeka et al. (2005a) and Bandyopadhyay et al. (2006) conducted in Nigeria and Ghana, respectively, underscores the epidemiological specificity of rugged landscapes. In the vast sedimentary or coastal plains (Benin, Nigerian basin), edaphic waterlogging operates as the quasi-exclusive epidemic driver, justifying the large-scale application of uniform phytosanitary recommendations. Conversely, our study demonstrates that in a contrasted relief such as western Côte d'Ivoire, this epidemic linearity is broken. Local hydromorphy does not alone govern disease intensity: it is its strict intersection with the regional thermal gradient that determines its expression, spatial distribution and aetiological composition.

The impact of the thermal gradient translates into a profound restructuring of the aetiological complex, characterised by a 'fungal niche inversion' resulting in the substitution of the dominant fungal species for a similar topographic position and hydric constraint. In the hot Cavally lowlands, *Sclerotium rolfsii* was involved in 98.2% of infection profiles, either alone or in co-infection with *Lasiodiplodia theobromae*, inducing rapidly progressing soft rots and severe losses (DSI = 2.00 ± 1.33). These observations align with the ecophysiological thresholds established by Ferreira et al. (2019) and Sangpueak et al. (2023), who confirm the requirement for temperatures above 25 °C for optimal mycelial development and sclerotial production of *S.*

rolfsii. Conversely, in the higher-altitude Tonkpi lowlands (> 300 m; approximately 24.0–24.5 °C), a similar waterlogging level translated into moderate severity (DSI = 0.81 ± 1.19) and a quasi-exclusive dominance of *Lasiodiplodia theobromae* (94.3%). This estimated regional thermal difference of 1.0–2.0 °C was thus sufficient to slow the kinetics of *S. rolfsii* to the benefit of *L. theobromae*, which is able to maintain its aggressiveness from 20 °C onwards (Machado et al., 2014). This restructuring of soil-borne communities along an elevational gradient is consistent with the observations of Lin et al. (2024) on soil pathogen ecology and falls within the interpretative framework of Bebber et al. (2013) on the redistribution of phytopathogenic fungi along isotherms.

The major influence of macroclimate on disease expression finds further confirmation in a second paradoxical phenomenon: the 'topographic risk inversion'. Indeed, our analyses reveal that the well-drained Cavally summits endured a significantly higher infection level (DSI = 0.46 ± 0.79; prevalence = 52.3%) than the Tonkpi slopes (DSI = 0.23 ± 0.53; prevalence = 31.4%), even though the latter are located in a physiographic position theoretically more exposed to run-off and water accumulation. This finding invalidates the unifactorial reading according to which local topographic position alone determines the sanitary vulnerability of a plot. It is consistent with the principles of landscape epidemiology outlined by Ostfeld et al. (2005), Plantegenest et al. (2007) and Savary et al. (2017), which posit that the intensity of an epidemic arises not from an isolated factor but from the complex intersection between edaphic drainage and regional thermal potential. In the hot lowlands, the elevated temperature largely compensates for the theoretical protection afforded by the good drainage of the summits, maintaining a significant infection pressure there.

This environmental modulation of risk directly calls into question the fixity of traditional agronomic benchmarks. The chronological harvest benchmark, empirically set at 12 months

after planting (MAP) in West Africa (Onyeka et al., 2005b), does not constitute a universal biological constant but an ecologically contingent median value. Indeed, the early-warning threshold (DSI > 0.5) was crossed as early as 8 MAP in the hot Cavally lowlands. This rapid disease progression warrants strict preventive management, allowing growers to anticipate harvest before reaching a level of irreversible commercial damage. This divergence is accompanied by a strengthening of the age–severity coupling, Spearman's coefficient (ρ) shifting from 0.212 on the Tonkpi summits to 0.868 in the Cavally lowlands. Far from contradicting the work of Onyeka et al. (2005b), these results confer upon it a landscape dimension that its original protocol, conducted in a homogeneous environment, could not reveal (Madden et al., 2007).

From an agronomic standpoint, our results allow the empirical 12-month benchmark to be replaced by a spatialised decision-making model (Fig. 5). This scheme adjusts the harvest calendar to the level of hydrothermal risk: emergency early uprooting (≤ 8 MAP) in the hot lowlands to avoid massive losses, a classical window (9–14 MAP) on transitional slopes, and prolonged standing storage (> 15 MAP) on the cool summits, effective refuge zones. Faced with the limits of fungicide efficacy (Ma & Michailides, 2005; Hollomon, 2015), this topo-altitudinal modulation offers growers a robust agroecological alternative, requiring no additional chemical inputs and mobilising solely growers' organisational resources.

These results must, however, be interpreted in the light of three methodological limitations. The exclusive use of vernacular names prevented isolating the share of resilience attributable to the intrinsic genetic tolerance of the cultivars. Secondly, fungal characterisation relied on morpho-cultural criteria, a classical approach but one that cannot discriminate cryptic species within the *Lasiodiplodia* and *Fusarium* complexes, whose resolution requires sequencing of the ITS and TEF1-α loci (Crous et al., 2009; Machado et al., 2014). Finally, the cross-sectional approach

adopted does not capture the interannual variability of hydrothermal regimes. These limitations call for two priority extensions: coupling molecular barcoding with continuous in situ microclimatic monitoring (Hohenfeld et al., 2024), and testing the interannual stability of the epidemiological thresholds identified here. Above all, in a context of global warming, the progressive shift of isotherms towards higher altitudes could favour the migration of *Sclerotium rolfsii* into areas currently preserved by the cold. This eventuality makes the multi-year evaluation of the temporal stability of these epidemiological thresholds essential to guarantee, in the long term, the sanitary resilience of the cassava sector.

5. Conclusion

This study demonstrates that the severity of cassava root rots in the humid tropics arises from a complex synergy between local edaphic hydromorphy and the regional thermal gradient. By articulating these factors at the scale of the agricultural landscape, this study substantially advances current understanding of this pathosystem around three major advances. Firstly, a small regional thermal gradient, estimated at 1.0–2.0 °C, is sufficient to reorganise the aetiological complex in the hydromorphic zones, driving a 'fungal niche inversion' between the dominance of *Sclerotium rolfsii* in the hot lowlands and that of *Lasiodiplodia theobromae* at higher altitudes. Secondly, the hot macroclimate of the lowlands erases the theoretical protection afforded by the good drainage of the summits, reveals a 'topographic risk inversion' that invalidates prediction models based solely on local topography. Finally, the chronological benchmark for the onset of the active epidemic phase (DSI > 0.5) is strongly shaped by the topo-altitudinal context. Crossed as early as 8 months after planting in the hot lowlands, this warning threshold is, in contrast, never reached on the cool high-altitude summits during the observation interval, thereby substituting for the uniform, non-spatialised 12-month chronological rule a harvest grid spatially calibrated to local vulnerability.

From an operational standpoint, these results equip agricultural extension services and growers with an accessible agroecological decision-making tool, based on plot position and plant age, to significantly mitigate the risk of irreversible commercial losses. As climate warming pushes isotherms towards altitudes currently spared, anticipating the migration of thermophilic pathogens such as *S. rolfsii* into these areas constitutes a strategic necessity to guarantee the sustainability of the sector and food security in the contrasted-relief zones of West Africa.

These advances nonetheless rest on morpho-cultural identifications whose molecular confirmation, planned as a follow-up, is required for the definitive taxonomic validation of the aetiological complex.

Acknowledgments The authors declare that no funds, grants, or other support were received during the preparation of this manuscript.

Declarations Competing Interests: The authors have no relevant financial or non-financial interests to disclose.

Author Contributions: Arthur Martin Affery, Yaya Toure, and Acka Emmanuel Dick conceived and designed the study. Material preparation, field surveys, and laboratory analyses were performed by Arthur Martin Affery, and Yaya Toure. Statistical modelling and data curation were conducted by Arthur Martin Affery and Yao Firmin N'Guessan. The first draft of the manuscript was written by Arthur Martin Affery. Acka Emmanuel Dick supervised the project and critically revised the manuscript. All authors reviewed and approved the final manuscript.

Data Availability: The datasets generated during and/or analysed during the current study are available from the corresponding author on reasonable request.

Ethics Approval: Not applicable. This study did not involve human participants or animals.

References

Bandyopadhyay, R., Mwangi, M., Aigbe, S.O. & Leslie, J.F. (2006) *Fusarium* species from the cassava root rot complex in West Africa. *Phytopathology* **96**(6), 673–676.

Banito, A., Kpémoua, K.E., Bissang, B. & Wydra, K. (2010) Assessment of cassava root and stem rots in ecozones of Togo and evaluation of the pathogen virulence. *Pakistan Journal of Botany* **42**(3), 2059–2068.

Bebber, D.P., Ramotowski, M.A.T. & Gurr, S.J. (2013) Crop pests and pathogens move polewards in a warming world. *Nature Climate Change* **3**, 985–988.

Brooks, M.E., Kristensen, K., van Benthem, K.J., Magnusson, A., Berg, C.W., Nielsen, A., Skaug, H.J., Maechler, M. & Bolker, B.M. (2017) glmmTMB balances speed and flexibility among applications of zero-inflated generalized linear mixed modeling. *The R Journal* **9**(2), 378–400.

Crous, P.W., Verkley, G.J.M., Groenewald, J.Z. & Samson, R.A. (2009) *Fungal biodiversity*. CBS-KNAW Fungal Biodiversity Centre.

FAO (2023) *FAOSTAT database: cassava production statistics*. Food and Agriculture Organization of the United Nations.

Ferreira, C.F., Alves, E., Guatimosim, E. & Oliveira, S.A.S. (2019) Ecology and pathogenicity of *Lasiodiplodia* species associated with cassava root rot in Brazil. *Phytopathology* **109**(7), 1125–1138.

Hillocks, R.J., Thresh, J.M. & Bellotti, A. (Eds) (2002) *Cassava: biology, production and utilization*. CABI Publishing.

Hohenfeld, C.S., Oliveira, S.A.S., Ferreira, C.F., Mello, V.H., Margarido, G.R.A., Passos, A.R. & Oliveira, E.J. (2024) Comparative analysis of infected cassava root transcriptomics reveals candidate genes for root rot disease resistance. *Scientific Reports* **14**, 10587.

Hohenfeld, C.S., Passos, A.R., Carvalho, H.W.L., Oliveira, S.A.S. & Oliveira, E.J. (2022) Genome-wide association study and selection for field resistance to cassava root rot disease and productive traits. *PLOS ONE* **17**(6), e0270020.

Hollomon, D.W. (2015) Fungicide resistance: 40 years on and still a major problem. In: Ishii, H. & Hollomon, D. (Eds) *Fungicide resistance in plant pathogens*, pp. 3–11. Springer, Tokyo.

ICAO (1993) *Manual of the ICAO Standard Atmosphere (extended to 80 kilometres)*, 3rd edn (Doc 7488). International Civil Aviation Organization.

Leslie, J.F. & Summerell, B.A. (2006) *The Fusarium laboratory manual*. Wiley-Blackwell.

Lin, Z., Halliday, F., Zhang, P., Wang, X., Chen, F., Shi, A., Shi, J., Xiao, Y. & Liu, X. (2024) Above- and belowground plant pathogens along elevational gradients: patterns and potential mechanisms. *Oikos* **131**(11), e10455.

Ma, Z. & Michailides, T.J. (2005) Advances in understanding molecular mechanisms of fungicide resistance and molecular detection of resistant genotypes in phytopathogenic fungi. *Crop Protection* **24**, 853–863.

Machado, A.R., Pinho, D.B., Oliveira, S.A.S. & Pereira, O.L. (2014) New occurrences of Botryosphaeriaceae causing black root rot of cassava in Brazil. *Tropical Plant Pathology* **39**(6), 464–470.

Madden, L.V., Hughes, G. & van den Bosch, F. (2007) *The study of plant disease epidemics*. APS Press.

McKinney, H.H. (1923) Influence of soil temperature and moisture on infection of wheat seedlings by *Helminthosporium sativum*. *Journal of Agricultural Research* **26**, 195–217.

Onyeka, T.J., Dixon, A.G.O. & Ekpo, E.J.A. (2005a) Identification of levels of resistance to cassava root rot disease (*Botryodiplodia theobromae*) in African landraces and improved germplasm using an in vitro inoculation method. *Euphytica* **145**(3), 281–288.

Onyeka, T.J., Dixon, A.G.O. & Ekpo, E.J.A. (2005b) Field evaluation of root rot disease and relationship between disease severity and yield in cassava. *Experimental Agriculture* **41**(3), 357–363.

Ostfeld, R.S., Glass, G.E. & Keesing, F. (2005) Spatial epidemiology: an emerging—or re-emerging—discipline. *Trends in Ecology & Evolution* **20**(6), 328–336.

Plantegenest, M., Le May, C. & Fabre, F. (2007) Landscape epidemiology of plant diseases. *Journal of the Royal Society Interface* **4**(16), 963–972.

Sangpueak, R., Duchanee, S., Saengchan, C., Papathoti, N.K., Phansak, P. & Buensanteai, N. (2023) Identification of cassava black stem and root rot agents in Thailand. *Chilean Journal of Agricultural Research* **83**(1), 70–82.

Savary, S., Bregaglio, S., Willocquet, L., Gustafson, D., Mason-D'Croz, D., Sparks, A., Castilla, N., Djurle, A., Allinne, C., Sharma, M., Rossi, V., Amorim, L., Bergamin, A., Yuen, J., Esker, P., McRoberts, N., Avelino, J., Duveiller, E., Koo, J. & Garrett, K. (2017) Crop health and its global impacts on the components of food security. *Food Security* **9**, 311–327.

Smithson, M. & Verkuilen, J. (2006) A better lemon squeezer? Maximum-likelihood regression with beta-distributed dependent variables. *Psychological Methods* **11**(1), 54–71.

SODEXAM (2021) Climatological standard normals 1990–2020 for Côte d'Ivoire. Société d'Exploitation et de Développement Aéroportuaire, Aéronautique et Météorologique, Abidjan, Côte d'Ivoire.

UNESCO (2024) *Les savoir-faire liés à la fabrication de l'attiéké en Côte d'Ivoire* [Know-how related to the production of attiéké in Côte d'Ivoire]. Representative List of the Intangible Cultural Heritage of Humanity, 19.COM.

Vilas Boas, S.A., Oliveira, S.A.S., Bragança, C.A.D., Ramos, J.B. & Oliveira, E.J. (2017) Survey of fungi associated with cassava root rot from different producing regions in Brazil. *Scientia Agricola* **74**(1), 60–67.

Zinsou, V.A., Afouda, L.A.C., Ahohuendo, B.C. & Wydra, K. (2017) Importance of fungal root rot pathogens of cassava in Benin. *Pakistan Journal of Botany* **49**(5), 2023–2028.

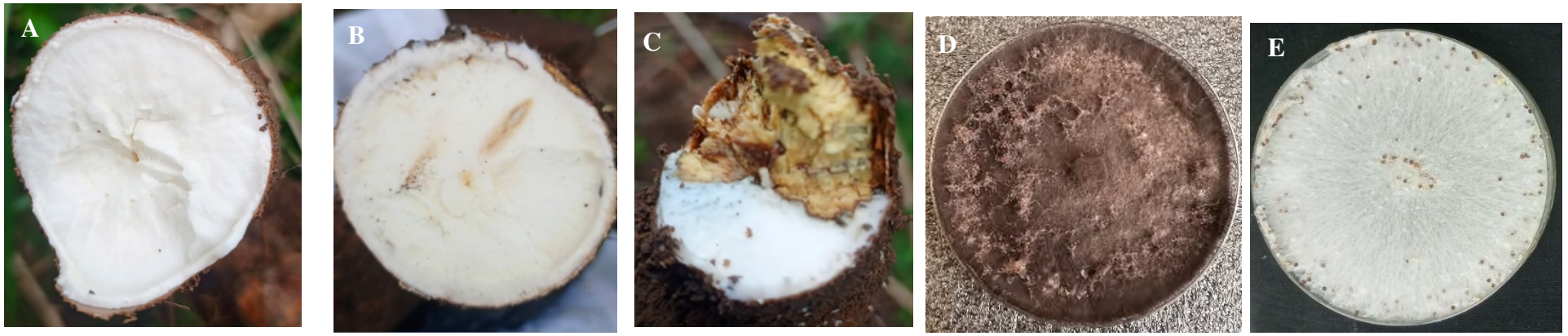

Fig 1. Representative stages of root-rot progression on a cassava root cross-section and predominant fungal agents in the Montagnes District, western Côte d'Ivoire.

(A) Healthy root (stage 0). (B) Early infection (stages 1–2). (C) Total destruction of the root system (stage 4). (D) Pure culture and sporulation of Lasiodiplodia theobromae. (E) Microscopic observation of Sclerotium rolfsii ('mustard-seed' sclerotia).

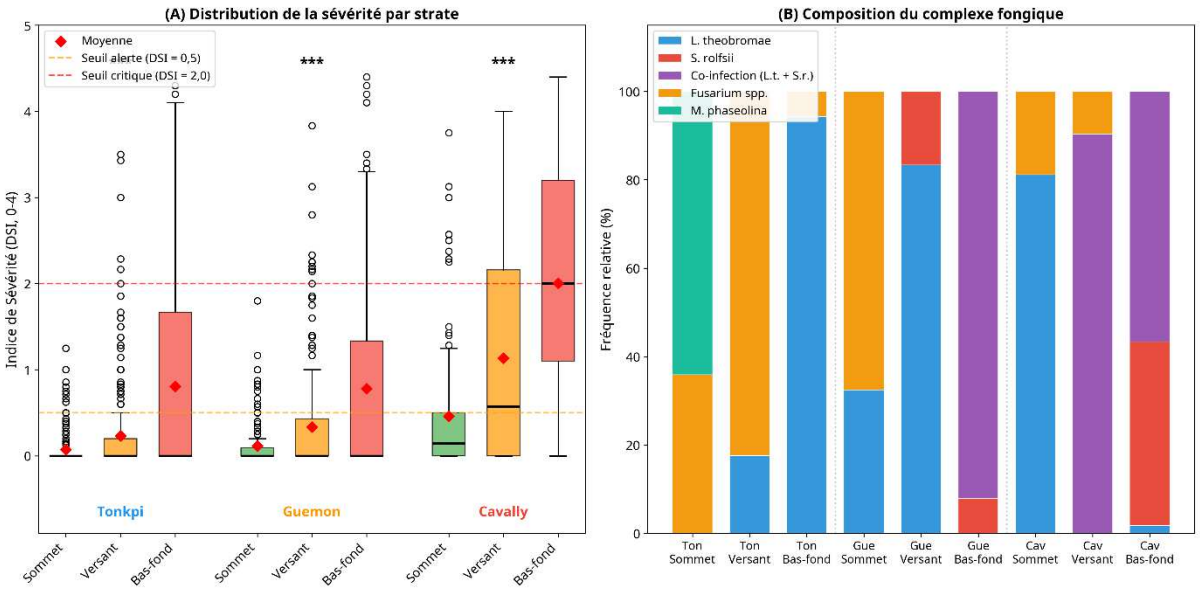

Fig 2. Severity of rots and frequency of soil-borne fungi in cassava roots in the Montagnes District, Côte d'Ivoire.

*(A) Distribution of the Disease Severity Index (DSI) along the toposequence for each region (red diamonds = means; *** $p < 0.001$). (B) Relative frequency of dominant pathogens per stratum. The aetiological complex undergoes an abrupt transition, shifting from a quasi-exclusive dominance of L. theobromae in the high-altitude massifs (Tonkpi) to a major dominance of S. rolfsii in the hot lowlands (Cavally).*

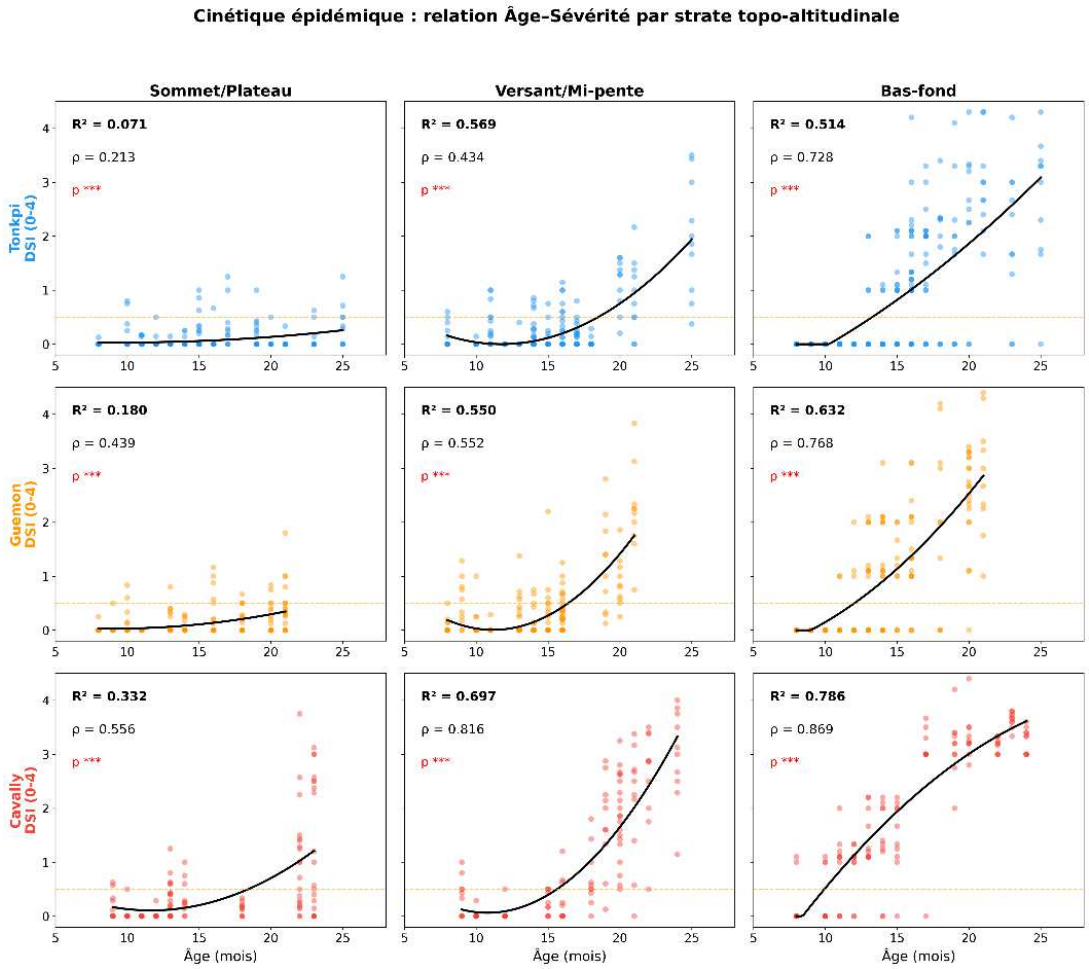

Fig 3. Modelling of the age–severity (DSI) relationship stratified by Region × Toposequence.

*Second-degree polynomial modelling (black curves) of the Disease Severity Index (DSI) as a function of plant age (months after planting). The orange dashed line indicates the early-warning threshold (DSI = 0.5), corresponding to entry into the active epidemic phase. For each stratum, the strength of the coupling is quantified by the coefficient of determination (R^2) and Spearman's rank correlation (ρ). Statistical significance: *** $p < 0.001$.*

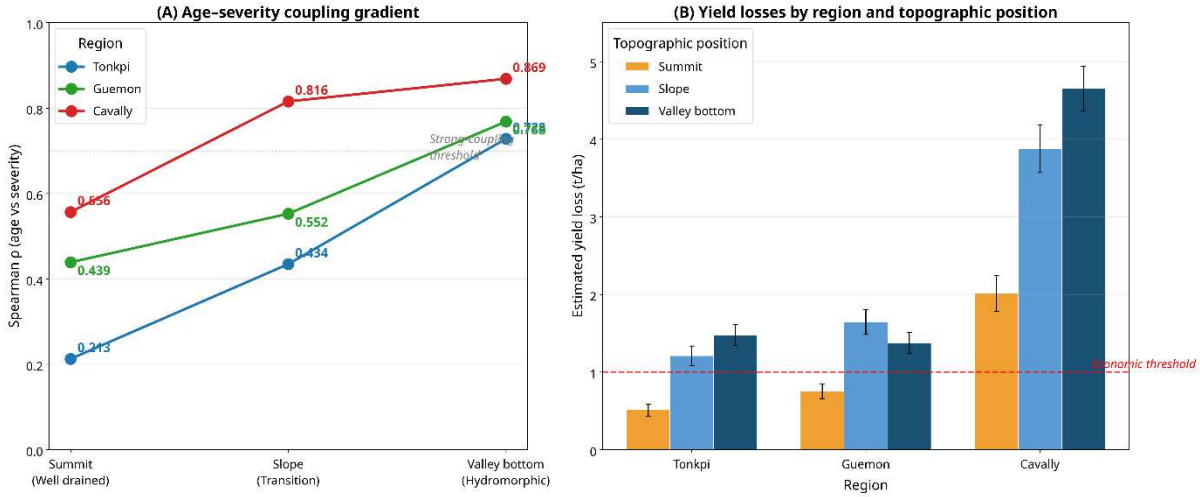

Fig 4. Age–severity coupling gradient and yield losses per topo-altitudinal stratum.

(*A) Evolution of Spearman's coefficient (ρ) between age and severity (DSI) along the toposequence. The horizontal dashed line indicates the strong-coupling threshold (ρ = 0.7). (B) Estimated yield losses (t ha*$^{-1}$*, reference yield = 10 t ha*$^{-1}$*) by region and topographic position. The red dashed line indicates the economic threshold (1 t ha*$^{-1}$*). The yield deficit intensifies along the gradient, reaching its maximum in the Cavally lowlands.*

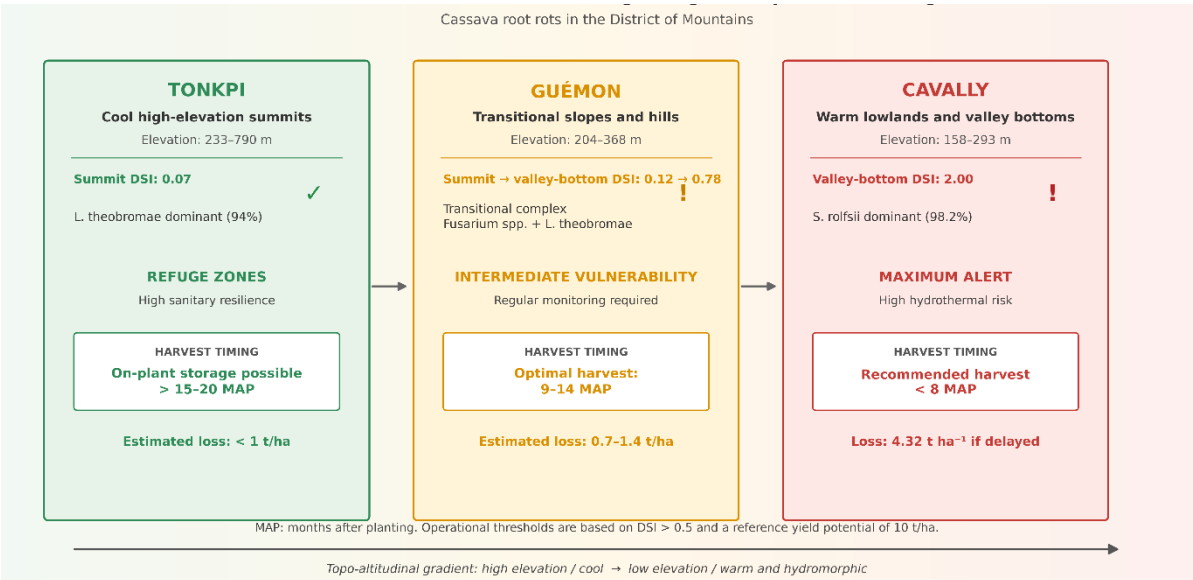

Fig 5. Spatial decision-making model for cassava harvest timing along the topo-altitudinal hydrothermal gradient in the Montagnes District.

Schematic representation of the three agronomic intervention windows identified in the Montagnes District:

(Zone 1) the maximum-alert zone (hot lowlands of Cavally), requiring harvest at or before 8 months after planting (MAP), as soon as the first visible epidemic signs appear, in order to prevent irreversible commercial losses linked to root-rot progression; (Zone 2) the intermediate-vulnerability zone (transition slopes and hills of Guémon), with a classical uprooting window at 9–14 MAP; and (Zone 3) the refuge zones (cool high-altitude summits of Tonkpi), allowing prolonged standing storage (> 15–20 MAP) with a negligible marketable deficit (< 1 t ha^{-1}).

Supplementary Files

This is a list of supplementary files associated with this preprint. Click to download.

- Table1.docx
- Table2.docx
- Table3.docx